CHAPTER 217

DYNAMIC BEHAVIOR OF A MOORING BUOY INSTALLED IN OPEN SHORE

TOSHIYUKI SHIGEMURA*, M.ASCE
AND
KENJIRO HAYASHI**

Abstract

To investigate the dynamic behavior of a mooring buoy installed in an open shore, a simplified simulation model is developed, which consists of the surging and heaving motions of a mooring buoy.

A series of the model tests is performed to examine the reliability of the developed model. The model tests verify that the developed model can predict the dynamic motion of a mooring buoy satisfactorily.

Finally, simulation is made for the buoy installed in the west shore of Iwo-jima which failed during a stormy weather. This simulation indicates that the external loads enough to cause the failure has been loaded on the buoy at the moment of the failure.

Introduction

A mooring buoy is normally installed inside a port or a bay where it is well protected against severe wind and wave loads. However, on some shores where a port can't be built for some reason, it has to be installed in the open shore where it is fully exposed to severe environmental condition. Iwo-jima is an example of this.

Iwo-jima is an isolated small volcanic island located in the Pacific Ocean about 1250 kilometers south of Tokyo. Because of the continuous upheaval of the island, no port has been built there yet. Instead, four single point mooring buoys have been installed off the west shore of the island, to moor the tankers or cargo ships which occasionally come to the island. The problem experienced by these mooring buoys is the frequent failures of the buoy systems during a period of stormy weather although no ship is moored to the buoys. In fact, the mooring buoys installed in Iwo-jima often fail during the typhoon season, which causes a lot of trouble for the supplying operation to the island.

Thus, to insure efficient operation of the mooring buoys installed in the open sea, it is important to clarify the

---

*Professor, Department of Civil Eng., National Defense Academy, 1-10-20 Hashirimizu, Yokosuka, Kanagawa 239, Japan.
**Assistant Professor, Department of Civil Eng., National Defense Academy.

dynamic behavior of the mooring buoys to which no ship is moored. This paper intends to investigate the dynamic behavior of a single point mooring buoy when no ship is moored to it. The investigation will be performed by putting the emphasis on the research of tensile stress induced on a mooring line as follows:
(1)Development of a simplified simulation model of a single point mooring buoy subject to severe environmental loads.
(2) Examination of the adequacy of the developed model through the model tests.
(3) Investigation of the possible causes of a failure which occurred in Iwo-jima through the simulation done by using the developed model.

Motion Equations of a Mooring Buoy

When a ship is not moored to a buoy, the buoy may experience the translational motions called surging, swaying and heaving and the rotatory motions called rolling, pitching and yawing due to the environmental loads. Thus, six equations should be developed and solved simultaneously to clarify the dynamic behaviors of the mooring buoy. However, it is difficult at the present stage to get reliable equations which represent each of these six motions. Further, one of the aims of this paper is to develop a simplified simulation model which can predict the dynamic behaviors of the tensile stress induced on a mooring line satisfactorily. Thus, the following assumptions were made to derive the motion equations:
(1) A mooring buoy doesn't take any rotational motions but takes the translational motions of surging and heaving.
(2) Dynamic motion of the mooring line is not taken into account in the derivation of the simulation model.
(3) A buoy is moored to the sea floor by an open link chain of uniform size which is elastically extensible.
(4) Only the wind and wave loads act on a buoy as the external loads.
(5) Tensile stress induced on the line by external loads can be substituted for the static tensile stress evaluated by an available formula.

Assumption (1) means that the motion of a mooring buoy can be treated as a two dimensional motion. Figure 1 shows the coordinate system used for deriving the motion equations. Here, each notation in figure 1 indicates the following:
a=draft of the buoy
b=freeboard of the buoy
F_{wd}=wind load acting on the buoy
T=tensile stress induced on the mooring chain
T_x=horizontal component of T
T_z=vertical component of T
F_x=horizontal component of the wave load acting on the buoy
F_z=vertical component of the wave load acting on the buoy
η=elevation of wave surface

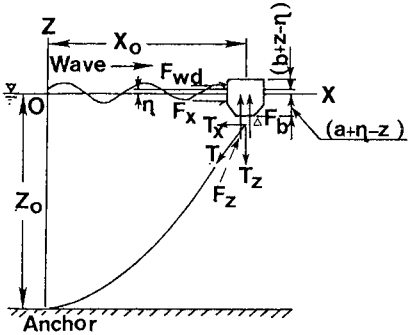

Figure 1. Coordinate system used for the analysis.

X_o=original position of the model buoy on X axis
Z_o=original position of the model buoy on Z axis

Suppose the model buoy moved to (X_o+x, Z_o+z) from its initial position (X_o, Z_o) for time t due to the wind and wave load. Then, basing on the assumptions together with the coordinate system provided, the following two equations can be derived as the motion equations of a mooring buoy:

$$(m+m'_x)\ddot{x}=F_{wd}+F_x-T_x-C_x\dot{x} \quad .....(1)\text{(for surging)}$$

$$(m+m'_z)\ddot{z}=F_z-T_z+\Delta F_b-C_z\dot{z} \quad .....(2)\text{(for heaving)}$$

where
m=mass of a buoy
$m'_{x,z}$=horizontal and vertical components of virtual mass of model buoy
$C_{x,z}$=horizontal and vertical components of damping coefficient of a buoy system
ΔF_b=dynamic buoyance of model buoy
X=horizontal displacement of a buoy from the origin
x=horizontal displacement of a buoy from its initial position
Z=vertical displacement of a buoy from the origin
z=vertical displacement of a buoy from its initial position

The former equation includes the horizontal components of wind load F_{wd} and wave load F_x, both acting on a buoy, tensile force induced on a chain T_x, and a damping force of the buoy system $C_x dx/dt$. The latter includes the vertical components of the wave load F_z, tensile stress T_z, damping force of the buoy system $C_z dz/dt$, and the dynamic buoyance of the buoy ΔF_b. However, values of these components together with the coefficient values are all unknown and should be somehow determined at an arbitrary time to solve eqs.(1) and (2) simultaneously.

Evaluation of Tensile Stress and External Loads

The catenary theory is generally used to calculate the static tensile stress induced on a mooring line. However, the value of the tensile stress T varies due to the hanging state of a mooring line under the water. The hanging state is usually classified into three states as follows:
(1) State I in which a part of the mooring line is hanging down vertically from a buoy to the sea floor and the rest of it is resting on the sea floor.
(2) State II in which the most part of the mooring line is hanging in the water forming a catenary curve although the rest of the chain is resting on the sea bed near the anchor.
(3) State III in which all of the mooring line is suspended in the water and no part of the line is resting on the sea bed near the anchor.

Figure 2 shows these states of the hanging of a mooring line. The notations in this figure indicates the following:
X_1=limiting displacement of a buoy from its origin in which the hanging state of the mooring line stays in state I.
X_2=limiting displacement of a buoy from its origin in which the hanging state of the mooring line stays in state II.
X_3=limiting displacement of a bouy from its origin in which the hanging state of the mooring line stays in state III.

a_r=length of the mooring line resting on the sea floor.
θ_a=directional angle of the tangential line to the mooring line at the anchoring point measured from the sea floor.

Calculation of the tensile stress is then made for each of these three states separately. Shoji(1975) introduced the effect of the elasticity of a mooring line to the catenary theory and derived three approximate polynomials expanded into a power series of T_x. However, there is some uncertainty in his equation for the line in state II. Further, there is some difficulty in finding the real value of T_x among the solutions of the polynomials. Thus, the authors developed new equations for each of the three states (1987), following Shoji's deriving method. Table 1 summarizes these equations developed for each state of hanging.

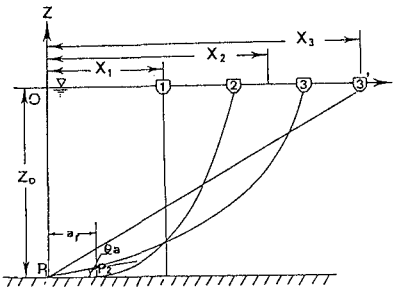

Figure 2. Hanging states of a mooring lines.

Table 1. Summary of the equations for evaluating the tensile stress induced on a mooring line and other related terms

Equations for a mooring line in State I

$$T_x=0 \quad \text{.....(3)}$$

$$T_z=W\,Z_o-WZ_o^{\,2}/(2EA) \quad \text{.....(4)}$$

$$X_1=S-Z_o+WZ_o^{\,2}/(2EA) \quad \text{.....(5)}$$

Equations for a mooring line in State II

$$X=S(1+T_x/EA)-(S-a_r')+T_x/W\left\{\ln W/T_x(S-a_r')+\sqrt{\left[W(S-a_r')/T_x\right]^2+1}\right\} \quad \text{.....(6)}$$

$$Z_o=\sqrt{(T_x/W)^2+(S-a_r')^2}-T_x/W+W(S-a_r')^2/(2EA) \quad \text{.....(7)}$$

$$T_z=W(S-a_r') \quad \text{.....(8)}$$

$$X_2=T_xS/EA+T_x/W\left\{\ln WS/T_x+\sqrt{(WS/T_x)^2+1}\right\} \quad \text{.....(9)}$$

Equations for a mooring line in State III

$$X=T_xS/EA+T_x/W\left\{\ln\left[\tan\theta_a+WS/T_x+\sqrt{(\tan\theta_a+WS/T_x)^2+1}\right]-\ln\left[\tan\theta_a+\sqrt{\tan^2\theta_a+1}\right]\right\} \quad \text{.....(10)}$$

$$Z_o=T_x/W\left\{\sqrt{(\tan\theta_a+WS/T_x)^2+1}-\sqrt{\tan^2\theta_a+1}+WS(\tan\theta_a+WS/2T_x)/EA\right\} \quad \text{.....(11)}$$

$$T_z=T_x\tan\theta_a+WS \quad \text{.....(12)}$$

$$X_3=\sqrt{S^2-Z_o^{\,2}} \quad \text{.....(13)}$$

In this table, several new notations appear. These notations indicate the following:
S=total length of a mooring line before getting deformation
W=weight of a mooring line per unit length under the water
A=sectional area of a mooring line
a_r'=original length of a_r before getting a deformation
Using these equations developed above, we can determine the static tensile stress and its components induced on a mooring line for any location of buoy if the physical properties of the mooring line are given. Namely, the values of T_z and X_1 are determined immediately from eqs.(4) and (5) because every variable in the equations is known. In case of State II, values of T_x and T_z can be determined from eqs.(7) and (8) if a_r' is given. Once the value of T_x is determined, the corresponding X_2 is also determined from eq.(6). In case of State III, the values of T_x and T_z are determined similarly from eqs.(11) and (12) if the value of $\tan\theta_a$ is given. The corresponding value of X is then determined from eq.(10) easily.

Next, let's derive the equations for wind and wave loads, referring to figure 1. It was decided to evaluate the wind load F_{wd} by a conventional type formula as shown below.

$$F_{wd}=1/2\rho_a C_d D(b+Z-\eta)V^2 \quad \text{.....(14)}$$

where ρ_a is air density, C_d is drag coefficient of a buoy, D is diameter of a buoy, b is freeboard of a buoy, η is the elevation of wave surface, z is the elevation of the gravity center of the buoy and V is the mean velocity of wind. Further, it was assumed that wave load can be evaluated by the following formulas derived from the Morison equation:

$$F_x=1/2\rho_w C_{dx} D(a+\eta-z)u|u|+1/4\rho_w C_{mx} D^2(a+\eta-z)\dot{u} \quad \text{....(15)}$$

$$F_z=1/8\rho_w C_{dz} D^2 v|v|+1/4\rho_w C_{mz} D^2(a+\eta-z)\dot{v} \quad \text{.....(16)}$$

where
ρ_w=water density
u=horizontal component of water particle's velocity at still water level
$\dot{u}$=horizontal component of water particle's acceleration at still water level
C_{dx}=drag coefficient of a buoy for horizontal flow
C_{mx}=mass coefficient of a buoy for horizontal flow
v=vertical component of water particle's velocity at still water level
$\dot{v}$=vertical component of water particle's acceleration at still water level
C_{dz}=drag coefficient of a buoy for vertical flow
C_{mz}=mass coefficient of a buoy for vertical flow

Finally, it was decided to evaluate the dynamic buoyance ΔF_b by the following equation:

$$\Delta F_b=1/4\ \rho_w D^2(a+\eta-z) \quad \text{.....(17)}$$

Using the equations developed above, respective terms in the righthand sides of eqs.(1) and (2) could be evaluated once we get the values of respective coefficients, flow field induced by the wave, physical properties of the buoy

and mooring line, and other values of the related terms.

Model Tests of a Single Point Mooring Buoy

As described previously, a mooring buoy installed off the west shore of Iwo-jima often fail during the typhoon season. Photo 1 shows the failure which occurred at Iwo-jima on August 4, 1986. In this case, the mooring chain was parted due to the severe environmental loads caused by the typhoon and the buoy was cast on the west coast of the island.

Photograph 1. Buoy cast on the west coast of Iwo-jima.

Thus, it was decided to perform a series of model tests in light of the buoy systems and their surrounding environmental conditions at the west shore of Iwo-jima. The following basic principles were established for performing the model tests:

(1) Model tests are to be performed in a two dimensional wave tank with a constant depth of water.
(2) Regular waves of various size will be used as the waves acting on the buoy.
(3)A constant weight will be loaded on the buoy horizontally instead of blowing wind at the bouy.
(4)An open link chains will be used as the mooring line because of its availability, although stud link chains are used in Iwo-jima.

The geometric scale of the test model was set to be 1/35 of the prototype and the time scale was determined by referring to the Froude law of similarity. Table 2 summarizes the detail of the test conditions.

Table 2. Details of the model tests

Dimension of the model buoy	
Diameter	7.9 cm(2.76 m)
Height	5.2 cm(1.83 m)
Draft	2.4 cm(1.0 m)
Weight in the air	70.0 grf(3.0 tonf)
Dimension of the model chain	
Diameter	1.9 mm(68.0 mm)
Weight under the water	0.7 grf/cm(86.5 kgf/m)
Length	57.1 cm(20.0 m), 68.6 cm(24.0 m), 91.4 cm(32.0 m), 114.3 cm(40.0 m)
Type	Open link(Stud link)
Range of the test conditions	
Water depth	45.7 cm(16.0 m)
Wave height	3.0--16.5 cm(1.0--5.8 m)
Wave period	0.7 --2.0 s(4.1--11.8 s)
Steepness	0.01--0.10
Wind load	12.9 grf(55.0 m/s)
Scope of the mooring line	1.25, 1.50, 2.0 and 2.5

In this table, the numerical figures in parentheses indicate the corresponding values for the prototype in Iwo-jima.

The model buoy was made of aluminum. Chains of four different length were prepared to use as mooring line. The length of these chains was determined so that the scope of the line may become the respective values shown in table 2. Here, the scope is a parameter defined as the ratio of line length to the depth of water.

A 39.6m long, 0.6m wide and 0.8m high wave channel was used for the model tests. Around the middle portion of this channel, a model buoy was moored to the channel bottom by one of the four chains shown in table 2. Figure 3 shows the setup of the model test. A waterproof tension meter was placed on the line at the position just below the bottom of the model buoy, and string-pully system was provided upon the upper structure of wave channel so that constant weight may be loaded to the buoy horizontally through that system.

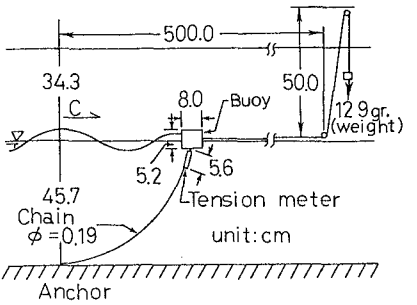

Figure 3. Setup of the model test

Beside the initial position of the buoy a capacitance type wave meter was installed and both the tension and wave meters were connected to a data recorder. Further, a video camera was placed in front of the buoy 2m from the glass wall to record the motion of buoy.

Regular waves of 24 kinds were chosen as the external waves acting on the buoy. Their characteristic values are shown in table 2. In addition, it was decided to load a constant weight of 12.9grf to the buoy horizontally as the substitute for the wind load. This weight of 12.9grf corresponds to the wind load which might be generated on the buoy by a wind having a speed of 55m/s. Here, the wind speed of 55m/s is the maximum one which was recorded in Iwo-jima for the past 20 years.

Prior to starting the model tests, performance of tension meter was examined statically. Tests were made in another small channel, changing both water depth and size of weight loaded on the model buoy horizontally through the string-pully system. The position of the model buoy, the size of the loaded weight, the hanging state of the mooring chain, and the tensile stress detected by the tension meter were all recorded. These tests were repeated a couple of times for three of the four chains prepared. The main tests were conducted for the model buoy moored by each of the four chains mentioned previously. This was done by exerting regular waves of 24 kinds one after another. In each run, both waves and tensile stress were recorded on the data recorder and the motion of the model buoy was recorded by video recorder.

Results of the Model Tests

To check the reliability of equations developed for evaluating the static tensile stress induced on the mooring line,

measured values of the horizontal components of tensile stress T_x were compared with the corresponding values calculated by the equations shown in table 1,using the physical properties of moorimg line shown in table 2. Further, it was assumed in the calculation that modulus of elasticity E_0 of the mooring line is 2.1×10^5 kgf/cm^2.

Figure 4 shows the results of this comparison. In this figure, CL means the length of the mooring line and D means the water depth at which the tests were made. As can be seen from this figure, calculated values of tensile stress agree quite satisfactorily with the measured ones within the range of the expected position of model buoy. This fact clearly verified that the developed equations would be quite reliable for evaluating the statical tensile stress induced on the mooring line.

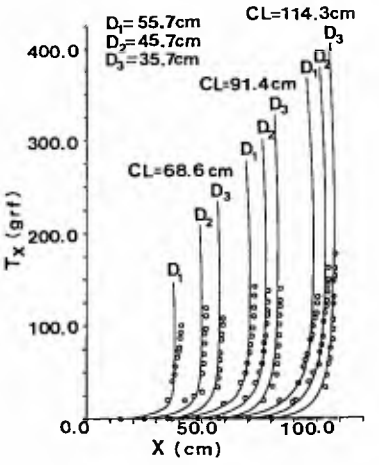

Figure 4. Reliability of the equations for evaluating the static tensile stress.

It was assumed previously that tensile stress induced on the mooring line dynamically could be substituted for the static tensile stress evaluated by some available equations. Thus, tensile stress T and its components T_x and T_z were all calculated similarly by the equations shown in table 1 by varying the position of the buoy every one centimeter within the expected range of the buoy's movement. This calculation was made for each of the four chains and the results were stored on floppy disks. Next, results of the model tests were analyzed. From the recorded data of tensile stress T, the extreme values of it were extracted from the record over 20 cycles, and their mean value T_m was determined by simply averaging them.

Photograph 2 is a picture of the orbital motion of model buoy. Similar pictures were taken at every run shading the laboratory from the sun light. At the same time, motion of the model buoy was recorded on a video recorder. Based on these data, the authors read the data such as horizontal and vertical displacements of model buoy x_m and z_m, the length of both major and minor axes of the inclined orbit of model buoy a_m and b_m, inclination of the major axis against the horizontal axis θ_{am} and the inclination of the mooring chain at the bottom of model buoy θ_{cm}. This data was analyzed using the steepness H_o'/L_o, ratio of wave height to water depth H/h of the

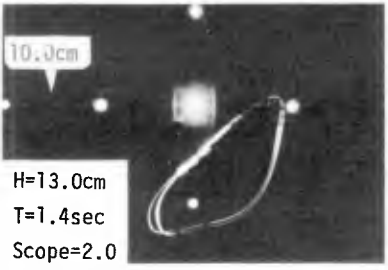

Photograph 2. Orbital motion of a buoy moored by a chain.

incident wave and scope of the mooring line as the controlling variables.

Figure 5 shows the relationship between T_m/W and H_o'/L_o plotted introducing the scope as a parameter. Here, W is the dead weight of model buoy. As can be seen from this figure, quite a high correlation exists between both variables. Further, it can be seen that the gradient between two variables decreases almost linearly as the value of scope increases.

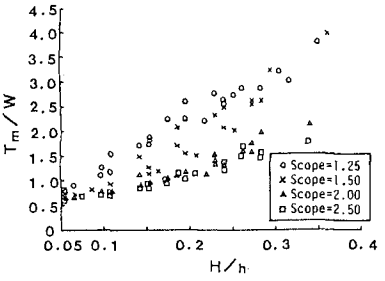

Figure 5. Relationship between T_m/W and H_o'/L_o.

Next, it was determined how the displacement of the buoy varies with the variation of external loads and mooring conditions. Figures 6 shows the relationship between x_m/L_o and H_o'/L_o. In this figure scope of the mooring line is taken as a parameter. From this figure, it can be seen that both x_m/L_o increases almost linearly as H_o'/Lo increases although the effect of the scope to the distribution is not clear. Similar distribution was also found between z_m/L_o and H'_o/L_o. Further, figure 7 shows the relationship between z_m/x_m and H_o'/L_o taking the scope as a parameter. Data scatters considerably. However, we can see that the ratio of both displacements tends to increase as H_o'/L_o increases in the range of H_o'/L_o less than approximately 0.3 and that it tends to have a constant value surrounding 1.0 in the range of H_o'/L_o greater than nearly 0.3. Effect of the scope is also not clear in this case.

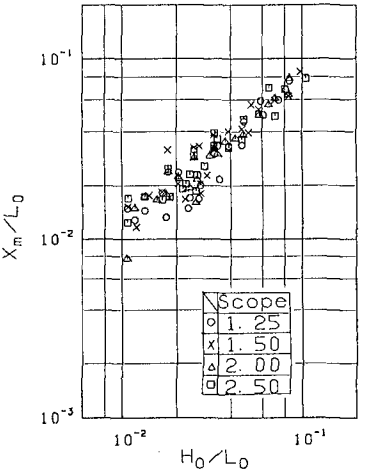

Figure 6. Relationship between x_m/L_o and H_o'/L_o.

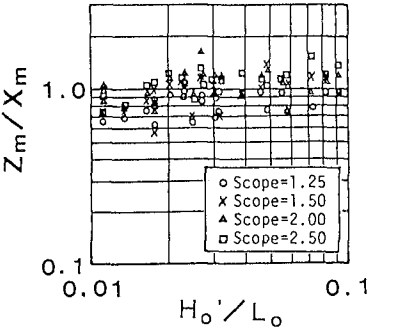

Figure 7. Relationship between z_m/x_m and H_o'/L_o.

Similar analyses were also made for the axial length of the inclined orbit of the buoy. Figure 8 shows the relationship between a_m/L_o and H_o'/L_o. From this figure, it can be seen that there exists a firm correlation between a_m/L_o and H_o'/L_o although the effect of the scope to this relationship is not seen clearly. Relationship between b_m/L_o and H'_o/L_o was also checked similarly. However, cor-

relation between b_m/L_o and H_o'/L_o was not as high as that found for a_m/L_o. Especially, in the range of H_o'/L_o less than 0.03, data of b_m/L_o scattered considerably against the corresponding values of H_o'/L_o.

Figure 9 shows the relationship between the ratio of both axial length a_m/b_m and H_o'/L_o. This figure shows that b_m/a_m tends to increase as H_o'/L_o increases in the range of H_o/L_o less than nearly 0.4 although data scatters considerably. Further, this ratio tends to converge to a constant value of nearly 0.05 in the range where H_o'/L_o is greater than approximately 0.05.

Finally, let's review the inclination of the mooring line at the bottom of model buoy. Figure 10 shows the relationship between θ_{cm} and H/h. In this case, scope of the mooring buoy is also taken as a parameter. As can be seen from this figure θ_{cm} tends to decrease almost linearly as the value of H/h increases in the range of H/h less than 0.25. This figure further indicates that θ_{cm} tends to keep a constant value of approximately 45 degrees in the range of H/h greater than 0.25.

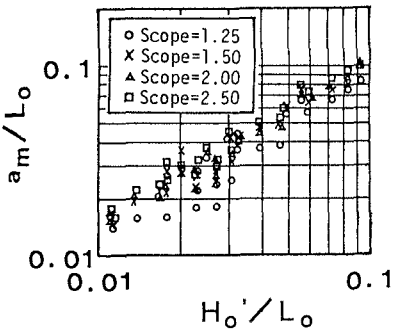

Figure 8 Relationship between a_m/L_o and H_o'/L_o.

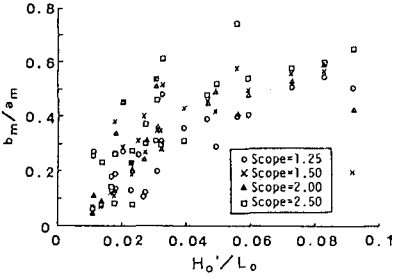

Figure 9. Relationship between a_m/b_m and H_o'/L_o.

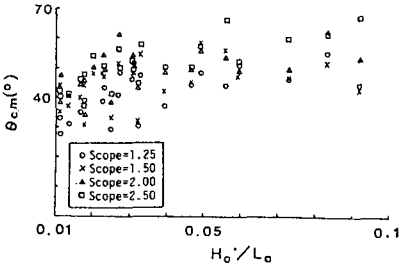

Figure 10. Relationship between θ_{cm} and H_o'/L_o.

Adequacy of the Simulation Model

The following assumptions were made prior to starting the numerical analysis:

(1) virtual mass of the model buoy m'_x and m'_z in eqs.(1) and (2) are both equal to the mass of water displaced by the model buoy.

(2) drag coefficients of model buoy C_{dx} and C_{dz} in eqs.(15) and (16) are both equal to 1.0.

(3) mass coefficients of model buoy C_{mx} and C_{mz} in eqs.(15) and (16) are both equal to 2.0.

(4) velocity and acceleration fields of the wave induced flow can be evaluated by the theory of small amplitude wave.

(5) damping coefficients of the buoy system C_x and C_z can be determined by trial and error method in the process of numerical analysis although the coefficient values determined

by Shoji(1975) through his tests of similar size are used as the initial values of them.

Based on these assumptions, we can now calculate the wave load and dynamic buoyance included in eqs.(1) and (2), for any time and location of model buoy. Further, wind load has been set to be 12.9grf and tensile stress and its components induced on the mooring line have been calculated for any location of model buoy. Thus, we are ready to solve eqs.(1) and (2) simultaneously. Numerical analyses were made for every case of the model tests by using the Runge-Kutter-Gill method. In the actual analyses, time interval was set to be 0.01 second and the analyses were proceeded until the calculated orbit of the model buoy reached almost stable state.

Figure 11 shows some examples of the numerical analyses. Namely, tensile stress T_c induced on the line and orbit of the model buoy both obtained from the analyses are compared in this figure with the corresponding ones measured in the model tests. The solid lines indicate the results obtained from the analyses and the dotted lines indicate the results measured in the model tests. From this figure, we can see that eqs(1) and (2) can simulate the dynamic motion of model buoy fairly well although the developed model tends to give a slight overestimation.

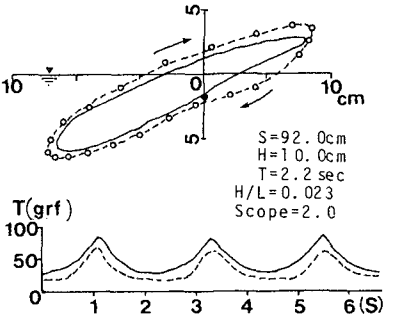

Figure 11. Example of the simulation of buoy's motion.

To see the adequacy of the simulation model more quantitatively, the maximum values of the calculated tensile stress T_c, horizontal and vertical displacements of model buoy x_c and z_c, and inclination of the mooring chain θ_{cc} were compared with the corresponding values measured through the model tests.

Figures 12 shows the distribution of T_c/T_m plotted against H_o'/L_o for the scope greater than 2.0. From this figure, we can see that developed model can predict the dynamic tensile stress induced on the mooring line quite satisfactorily when the scope value is greater than 2.0 and steepness of the acting wave is less than approximately 0.04. Further, the value of T_c/T_m scatters considerably when H_o'/L_o is greater than approximately 0.04. Similar analysis was made for the case whose scope is less than 1.5. In such a case, the developed model has a tendency to considerably overestimate the ten-

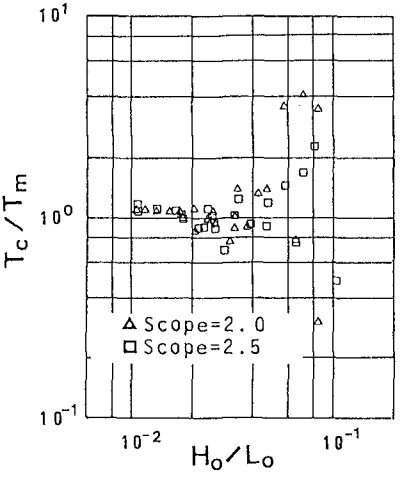

Figure 12. Relationship between T_c/T_m and H_o'/L_o.

sile stress.

Figures 13 shows the distribution of z_c/z_m plotted against H_o'/L_o. This figure indicates that z_c agrees quite satisfactorily with z_m in the whole range of H_o'/L_o used in this model test. However, the model still has a tendency to overestimate the respective displacements of the model buoy when the scope of the line is 1.25. Analysis done for x_c/x_m also indicates a similar distribution for the values of H_o/L_o.

Figure 14 shows the distribution of θ_{cc}/θ_{cm} plotted against H_o'/L_o. From this figure, we can see that θ_{cc}/θ_{cm} scatters around the value of 1.2 in the whole range of H_o'/L_o although the model has a tendency to overestimate θ_c.

These comparisons indicate that the developed model can trace the dynamic behaviors of the mooring buoy fairly well when scope of the mooring line is greater than 2.0 and the steepness of the acting waves is less than nearly 0.04. Further, these comparisons may indicate the possibility that the developed model can be improved more when some modifications are made on the values of respective coefficients and the formulae to evaluate wind and wave load.

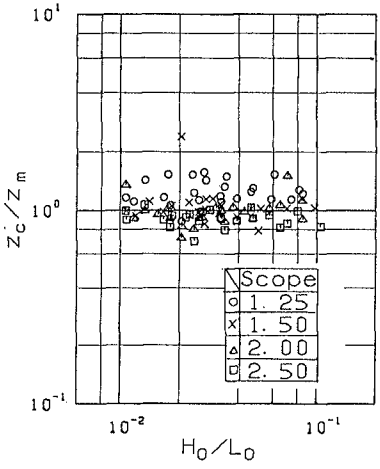

Figure 13. Relationship between z_c/z_m and H_o'/L_o.

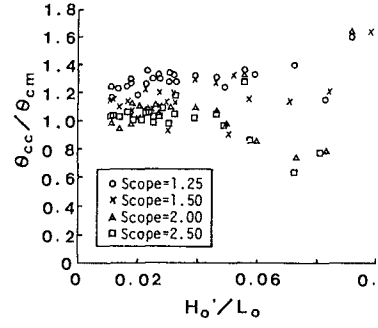

Figure 14. Relationship between θ_{cc}/θ_{cm} and H_o'/L_o.

Application of the Developed Model to a Real Buoy

To determine whether the developed model can be applied to simulate the dynamic behaviors of a real buoy, and further to see whether the simulation done by this model can serve to find any possible causes for the failures of buoy systems which have often occurred in Iwo-jima, it was decided to choose a failure incident which occurred in Iwo-jima on May 23, 1982, as an object of the simulation, and to simulate the dynamic behaviors of the buoy just before its failure.

This incident occurred during a stormy weather which was caused by the typhoon No.4 which had been hitting the island since the day before the failure. In this incident, the harp shackle was distorted seriously due to a huge tensile force induced on it by the severe environmental loads, and was pulled out through the chain hole of the buoy. As a result, the buoy was cast away on the west coast of the island. Figure 15 is the side view of a harp shackle of the

same size as that used at the island. As can be seen from this figure, it is clear that a huge tensile force strong enough to squash the shackle's width from 420 mm into 352 mm was loaded on it at the moment of the failure.

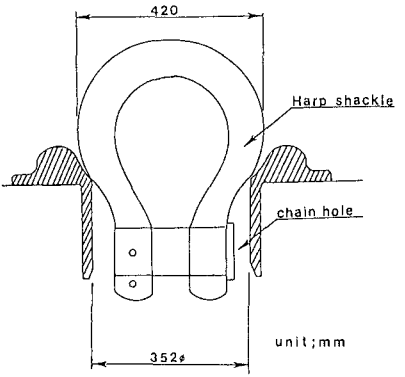

Figure 15. Side view of a harp shackle used in Iwo-jima in 1982.

Soon after the incident, the harp shackle was recovered by members of the Japan Maritime Self Defense Force (JMSDF) stationed there, and it was reported later that the width of the harp shackle was 364 mm and that several scratches were found on the inner wall of the chain hole of the recovered buoy. Further, the Engineering Office of JMSDF made a series of static pulling test of harp shackles in a laboratory and concluded that external loads of approximately 110 tonf were loaded on the harp shackle at the moment of the failure(1982). This buoy was one of four buoys installed off the west coast of Iwo-jima, and it had been just swapped two months before the incident. The depth of installation was 16m and, and the buoy had been moored by a 20 m long mooring chain with a diameter of 68mm. Thus, the scope of mooring line was 1.25. Just two weeks before the failure incident, the authors had installed a supersonic wave meter about 450 m off the west coast of Iwo-jima at a depth of 12 m(1984). This site is about 500 m south of the installation site of the four mooring buoys. Fortunately, the wave meter recorded the wave data for ten minutes every two hours during this typhoon although the wave meter was washed away by typhoon No.17 which hit the island in November, 1983.

Through the analysis of this record, it was found that the maximum wave height was nearly 7 m and the significant wave period was approximately 10 second. The JMSDF on Iwo-jima has a meteorological station which is built near the center of the island and whose elevation is approximately 110 m above the mean sea level. At 6 a.m. of May 23, 1982, the station recorded the instantaneous maximum wind speed of 26.0 m/s. However, wind data around the installation site of the buoy is unknown. Thus, it was decided to use the wind of 55m/s which is the maximum wind speed recorded on the island for the

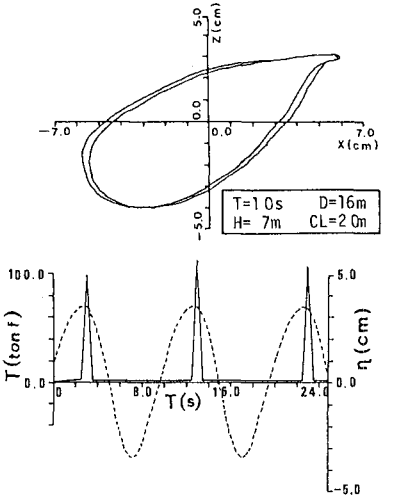

Figure 16. Results of the numerical analysis done for the buoy failed in Iwo-jima.

past 20 years. Further, it was decided to use the value of 1200 kgf.s/m for the damping coefficient C_x and the value of 560 kgf.s/m for the damping coefficient C_z, respectively. These values were determined by applying the Froude law of similarity to the corresponding coefficient values obtained through the model tests. Numerical analysis was made for the conditions stated above.

Figure 16 shows the analytical results. Namely, the upper figure shows the orbit of the buoy, and the lower one shows the time variations of both wave profile and tensile stress T. This figure clearly indicates that tensile stress exceeding 110 tonf may possibly be induced on the mooring line if the buoy is subject to as large external loads as those used for the numerical analysis.

Concluding Remarks

A rather simplified model was developed for simulating the dynamic behavior of a simple point mooring buoy which is installed in the open sea and the adequacy of the model was examined through the model tests. Further, using the developed model, numerical analysis was made for the dynamic motion of a real buoy in Iwo-jima whose system failed during a stormy weather caused by a typhoon. As a result, it was verified that the developed model can satisfactorily predict the dynamic behavior of a mooring buoy in the open sea.

References

1. Engineering Office of JMSDF,"Investigation report on the failure of No.1 buoy in Iwo-jima", p.13, June 1982.
2. Shigemura, T. and Komiya, Y.,"Formation of tombolo at the west coast of Iwo-jima",Proc. of the 19th Conf. on Coastal Eng.,Chap.96, pp.1403-1419, 1984.
3. Shigemura, T.,Hayashi, K and Kouzaki, T.,"Dynamic behavior of a single point mooring buoy installed in open shore", Proc. of the 34th Japanese Conf. on Coastal Eng., pp.621-625, 1987.
4. Shoji, K.,"Study on the motion of a moored buoy and tension of mooring lines", Journ. of the Society of Naval Architects of Japan, Vol.138, pp.233-246, 1975.